

SANDIA REPORT

SAND2015-1342
Unlimited Release
Printed Feb 2015

Impact of Materials Processing on Microstructural Evolution and Hydrogen Isotope Storage Properties of Pd-Rh Alloy Powders

Josh K. Yee, University of California, Davis

Prepared by
Sandia National Laboratories
Livermore, California 94550

Sandia National Laboratories is a multi-program laboratory managed and operated by Sandia Corporation, a wholly owned subsidiary of Lockheed Martin Corporation, for the U.S. Department of Energy's National Nuclear Security Administration under contract DE-AC04-94AL85000.

Approved for public release; further dissemination unlimited.



Issued by Sandia National Laboratories, operated for the United States Department of Energy by Sandia Corporation.

NOTICE: This report was prepared as an account of work sponsored by an agency of the United States Government. Neither the United States Government, nor any agency thereof, nor any of their employees, nor any of their contractors, subcontractors, or their employees, make any warranty, express or implied, or assume any legal liability or responsibility for the accuracy, completeness, or usefulness of any information, apparatus, product, or process disclosed, or represent that its use would not infringe privately owned rights. Reference herein to any specific commercial product, process, or service by trade name, trademark, manufacturer, or otherwise, does not necessarily constitute or imply its endorsement, recommendation, or favoring by the United States Government, any agency thereof, or any of their contractors or subcontractors. The views and opinions expressed herein do not necessarily state or reflect those of the United States Government, any agency thereof, or any of their contractors.

Printed in the United States of America. This report has been reproduced directly from the best available copy.

Available to DOE and DOE contractors from

U.S. Department of Energy
Office of Scientific and Technical Information
P.O. Box 62
Oak Ridge, TN 37831

Telephone: (865) 576-8401
Facsimile: (865) 576-5728
E-Mail: reports@adonis.osti.gov
Online ordering: <http://www.osti.gov/bridge>

Available to the public from

U.S. Department of Commerce
National Technical Information Service
5285 Port Royal Rd.
Springfield, VA 22161

Telephone: (800) 553-6847
Facsimile: (703) 605-6900
E-Mail: orders@ntis.fedworld.gov
Online order: <http://www.ntis.gov/help/ordermethods.asp?loc=7-4-0#online>



Impact of Materials Processing on Microstructural Evolution and Hydrogen Isotope Storage Properties of Pd-Rh Alloy Powders

J.K. Yee
University of California, Davis
Advanced Materials Research Laboratory
One Shields Ave
Davis, CA 95616

Abstract

Cryomilled Pd-10Rh was investigated as potential solid-state storage material of hydrogen. Pd-10Rh was first atomized, and then subsequently cryomilled. The cryomilled Pd-10Rh was then examined using microstructural characterization techniques including optical microscopy, electron microscopy, and X-ray diffraction. Pd-10Rh particles were significantly flattened, increasing the apparent surface area. Microstructural refinement was observed in the cryomilled Pd-10Rh, generating grains at the nanometric scale through dislocation-based activity. Hydrogen sorption properties were also characterized, generating both capacity as well as kinetics measurements. It was found that the microstructural refinement due to cryomilling did not play a significant role on hydrogen sorption properties until the smallest grain size (on the order of ~25 nm) was achieved. Additionally, the increased surface area and other changes in particle morphology were associated with cryomilling changed the kinetics of hydrogen absorption.

ACKNOWLEDGMENTS

JKY is extremely grateful for the support and opportunities provided by Sandia National Laboratories' Campus Executive Fellowship. The mentorship of Patrick Cappillino, Nancy Yang, Vitalie Stavila, and Chris San Marchi of Sandia National Laboratories, Livermore is also acknowledged.

CONTENTS

1. Introduction.....	7
2. Detailed description of experimental methods	8
3. Results.....	10
4. Discussion	18
5. Anticipated impact.....	24
6. Conclusions.....	25
7. References.....	27

FIGURES

Figure 1. Schematic of a typical cryomilling setup in service. The cryogenic liquid represented here is liquid nitrogen.	8
Figure 2. SEM micrographs of (a) as-atomized Pd-10Rh, and Pd-10Rh particles cryomilled for (b) 1h, (c) 2h, (d) 8h, (e) 16h, and (f) 16h BPR=64:1.....	10
Figure 3. SEM micrographs of cross-sections of (a) as-atomized Pd-10Rh, and Pd-10Rh particles cryomilled for (b) 1h, (c) 2h, (d) 8h, (e) 16h, and (f) 16h BPR=64:1.	11
Figure 4. TEM micrographs of (a) atomized Pd-10Rh particles, and Pd-10Rh particles that were cryomilled for: (b) 1 h, (c) 2 h, (d) 8 h, (e) 16 h, and (f) 16 h, BPR=64:1.	13
Figure 5. XRD patterns of atomized and cryomilled samples. Only the first five diffraction peaks are shown in this figure.	14
Figure 6. PC isotherms for as-atomized and cryomilled samples at (a) full range of molar H/M ratios and (b) low H/M ratios.....	16
Figure 7. H uptake kinetics for atomized and cryomilled Pd-10Rh samples.....	17
Figure 8. α_{\max} and θ_{\max} as a function of specific surface area.....	20
Figure 9. Comparison of α_{\max} and θ_{\max} as a function of dislocation density.....	21
Figure 10. Comparison of α_{\max} and θ_{\max} as a function of inverse grain size (nm^{-1}).	22
Figure 11. Comparison of specific surface area and hydrogen absorption half-life of atomized and cryomilled Pd-10Rh.	24

TABLES

Table 1. Powder and microstructural characteristics of atomized (as-atomized) and cryomilled Pd-10Rh powders (1h, 2h, 8h, and 16h refer to cryomilling times in hours). Crystallite size and microlattice strain determined from X-ray diffraction line profile analysis.	12
Table 2. Hydrogen uptake and solubility characteristics of atomized and cryomilled Pd-10Rh powders (1h, 2h, 8h, and 16h refer to cryomilling times in hours).....	17

1. INTRODUCTION

Within the last decade, there has been a strong driving force to study alternatives to hydrocarbons and associated technologies for energy applications due in part to the strong realization that these are not sustainable for the future. There are several technological and scientific issues, which must be overcome, and are currently of interest to various research communities. For hydrogen related technologies, one of the biggest challenges remaining is to understand different methods for storage until use. The most current method of hydrogen storage is through gas or liquid tanks; however, solid-state storage has many advantages to tank storage which include greater capacity and overall safety. Current Department of Energy criteria for hydrogen storage methods call for certain specifications regarding operating temperature, recharge/discharge rates, and overall capacity amongst others [1]. Several different materials are being evaluated for solid state hydrogen storage [2], including metallic hydrides, complex chemical hydrides, and mixed metal-organic framework materials (MOFs). Metallic hydrides are of particular interest because of their relative simplicity and overall high storage capacity in comparison to other metals. In order to fulfill some of these requirements for, a comprehensive understanding of fundamental phenomena surrounding hydrogen-material interactions must be obtained. For metallic hydrides, it is particularly important to understand the relationships between different microstructural defects (including free surfaces, grain boundaries, and dislocations) and hydrogen sorption behavior.

Of the various microstructural defects, which are present in materials, free surfaces, grain boundaries, and dislocations perhaps most strongly influence hydrogen behavior in various metal-hydrogen systems. From an intuitive perspective, the presence of free surfaces on a metal sample could strongly influence hydrogen sorption properties as hydrogen adsorption and disassociation on a surface is essentially the rate-limiting step of the hydrogen absorption process. The morphology of the free surface can also affect the adsorption process; however, the exact influence of certain types of defects (such as steps, ledges, etc.) does not seem to be well understood beyond that their presence can speed the rate of the reaction. Both grain boundaries and edge dislocations are well known to be potential hydrogen traps, which may in turn affect hydrogen sorption properties, particularly in terms of overall capacity and absorption rates.

Within the past 20-30 years, a new set of processing techniques have been developed to fabricate metals with high defect concentrations. This set of processing techniques, known as severe plastic deformation (SPD) techniques, uses a top-down processing approach where microstructure is developed through deformation of solid material [3]. Specific techniques, which belong to this set of processes include high pressure torsion (HPT), equal channel angular pressing (ECAP), and ball milling. During SPD processes, the material is plastically deformed, and dislocations are introduced into the microstructure. With increased deformation, more dislocations form and begin to move. The dislocations become entangled eventually forming dense dislocation walls. With further deformation, the dense dislocation walls transform into sub-boundaries within the grain. Increasing deformation transforms the sub-boundaries into low angle grain boundaries, and eventually high angle grain boundaries. This process continues to repeat itself on increasingly smaller length scales with increasing deformation. Additionally, vacancies are created in the microstructure when dislocations entangle and intersect to form jogs, emitting vacancies [4,5].

In the past, Yang and Lavernia [6] investigated the synthesis of palladium and palladium alloy powders through gas atomization, and the resulting hydrogen storage properties. They were able

to attribute some of the behavior, such as the sloping plateau phenomenon, to chemical inhomogeneity in the microstructure, which was caused through the gas atomization process. As an extension of their previous work, the present investigation studies the influence of a high concentration of defects, both on the mesoscale (such as particle morphology) and on the microscale (such as grain boundaries and dislocations), on hydrogen sorption properties of palladium alloys. Cryogenic milling, also commonly known as cryomilling, was selected as a method, which could be used to generate various defect concentrations into the powder. Cryomilling has been shown in several other investigations to be an effective method of introducing high volumes of defects, particularly grain boundaries, into structural materials like aluminum and titanium.

2. DETAILED DESCRIPTION OF EXPERIMENTAL METHODS

Previously, Yang and Lavernia created the first inert gas spray atomization unit for Pd and Pd alloys at the University of California, Irvine in the 1990s [7,6]. Further information on the process can be found in their SAND report. Pd-10Rh was selected as the composition of choice for this study, in part due to its ability to absorb large gravimetric quantities of hydrogen.

Three separate cryomilling experiments were performed in the course of this study. All experiments utilized a Union Process (Akron, Ohio) 1-S Svezgari-type attritor mill. A schematic of the cryomilling setup is shown in Figure 1.

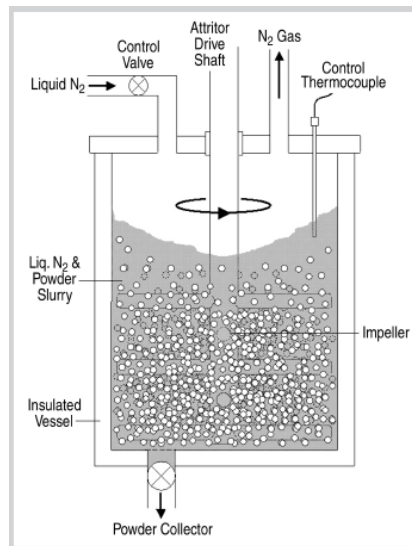


Figure 1. Schematic of a typical cryomilling setup in service. The cryogenic liquid represented here is liquid nitrogen.

The stainless steel milling vessel was modified to handle the input of cryogenic liquid, and the outgassing from the vaporization of the cryogenic liquid. The attritor speed was set at 180 RPM. The cryogenic liquid flow rate was maintained by an electronic controller, which monitored the liquid level using an electrically heated thermocouple. Stainless steel balls were used as the milling media. The first experiment utilized liquid argon as the cryogenic liquid, as well as a ball-to-powder ratio (BPR) of 32:1 (with a 1 kg powder charge). 2 g (0.2% wt.) of stearic acid was used as a process control agent (PCA) in order to prevent excessive cold welding of the

powder during the cryomilling experiment. The first cryomilling experiment lasted for 8 h, with intermediate powder collections occurring 1 and 2 h into the experiment. These intermediate collections were made in order to study the changes in the powder morphology at intermediate stages of the experiment. The second experiment also utilized a BPR of 32:1, and lasted for 16 h, and no intermediate samples were collected during this particular cryomilling experiment. The third and final cryomilling experiment utilized liquid nitrogen as the cryogenic liquid, and a BPR of 64:1 (500 g powder charge) for 16h. A higher BPR was used in order to increase the amount of deformation and refinement induced into the powder. No PCA was used in this cryomilling experiment, as the wettability of Pd-Rh to itself and the stainless steel fittings is poor and thus is not necessary to control cold welding.

The atomized and cryomilled Pd-10Rh powders were characterized using scanning electron microscopy (SEM), X-ray diffraction (XRD), and transmission electron microscopy (TEM). For the microstructural characterization, powder samples were prepared using conventional metallographic techniques. After mounting and polishing, cross-sections of the atomized and cryomilled Pd-10Rh powders were analyzed using a JEOL 7600 microscope (JEOL Ltd., Tokyo, Japan) operating at 15 kV. The XRD patterns were recorded on a PANalytical Empyrean X-ray diffractometer equipped with a PIXcel^{3D} detector and operated using Cu $K\alpha$ radiation ($\lambda = 1.5418$ Å). Scattering intensities were measured using the Bragg–Brentano (θ - 2θ) geometry over an angular range of $30^\circ < 2\theta < 120^\circ$ with a step size of 0.026° . Thin film samples for TEM were prepared using focused ion beam (FIB) in a FEI Dual Platform Helios NanoLab. TEM analysis was performed using a FEI CM30 at 300kV.

Surface area measurements (Brunauer, Emmett and Teller (BET) method) and pressure-composition (PC) isotherms were determined using a Micromeritics ASAP 2020 porosimeter. Samples were degassed for 15 hours at 50°C prior to surface area measurements using krypton gas at 77 K as the adsorbent. Krypton was used as the adsorbent gas to improve the resolution of the BET measurement because of the low surface area of the particles. Approximately 150 mg of powder was used in each of the hydrogen absorption experiments. Prior to hydrogen absorption experiments, sample surfaces were cleaned by three cycles of exposure to gaseous hydrogen gas at room temperature, each cycle consisting of hydrogen partial pressure of 8 Torr followed by evacuation. This surface cleaning procedure was used primarily to remove surface oxides (cleaning may also mitigate the potential surface effects of the liquid Ar exposure during cryomilling). For PC isotherm measurements, equilibrium was defined as changes in hydrogen pressure $< 0.01\%$ over 30 s intervals. Rates of hydrogen uptake were measured by loading the porosimeter manifold with gaseous hydrogen to pressure of ~ 900 Torr, opening the valve to the sample holder and recording the pressure drop at 25°C . After correction for near instantaneous expansion into the larger volume, pressure drop was converted to moles of hydrogen atoms and attributed to absorption by the Pd-10Rh alloy powder. The equilibrium (final) pressure after these uptake experiments varied between 510 and 530 Torr.

3. RESULTS

The as-atomized particles are spheroids in shape with a nominal diameter of approximately 20 μm , as shown in SEM images of the powder (Figure 2) and in cross section (Figure 3).

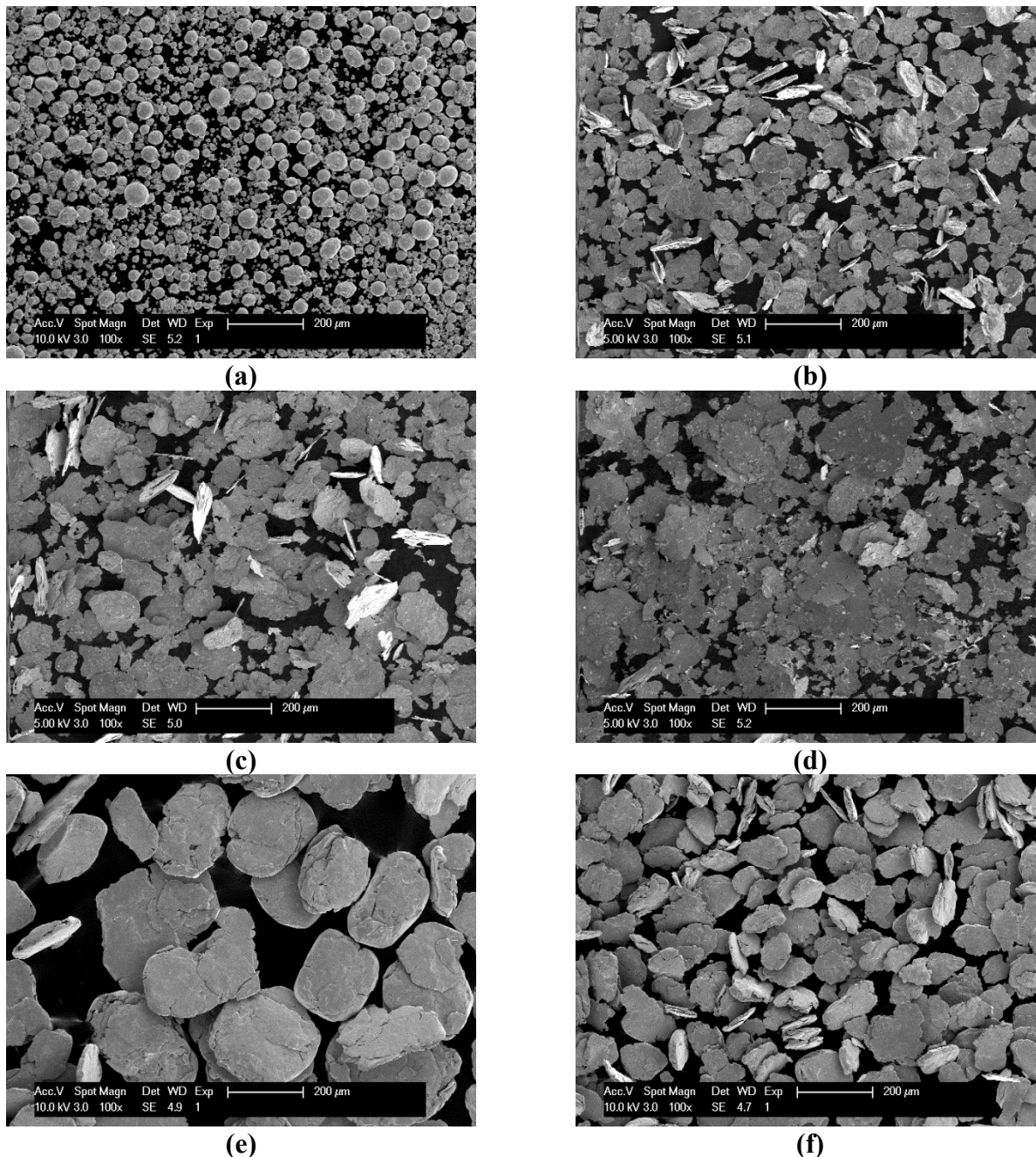


Figure 2. SEM micrographs of (a) as-atomized Pd-10Rh, and Pd-10Rh particles cryomilled for (b) 1h, (c) 2h, (d) 8h, (e) 16h, and (f) 16h BPR=64:1.

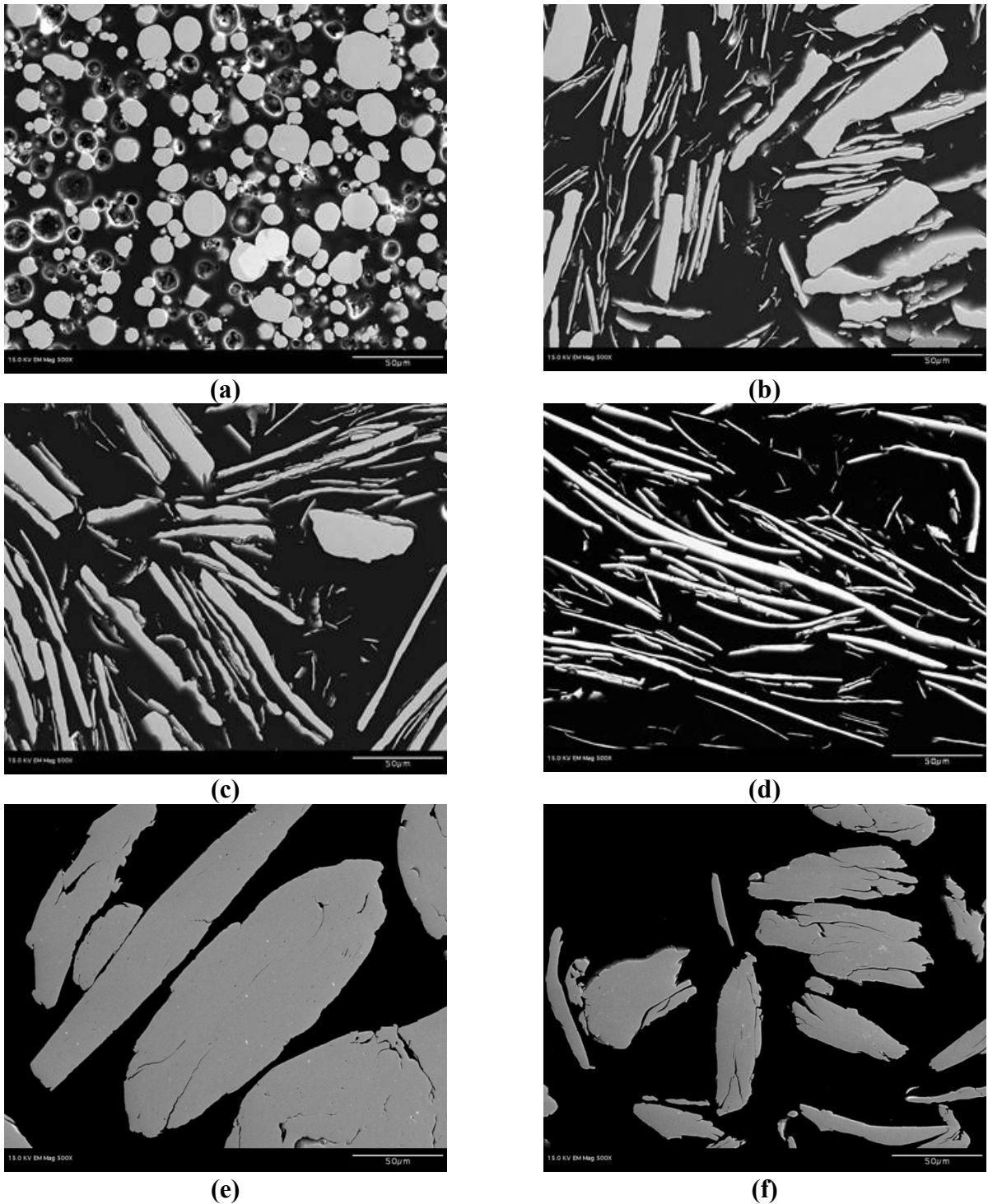


Figure 3. SEM micrographs of cross-sections of (a) as-atomized Pd-10Rh, and Pd-10Rh particles cryomilled for (b) 1h, (c) 2h, (d) 8h, (e) 16h, and (f) 16h BPR=64:1.

During cryomilling, the Pd-10Rh particle morphology evolved from the spherical as-atomized particles (with an aspect ratio near one) to high aspect-ratio, disk-shaped flakes with a diameter near 100 μm (Figures 2 b-d, 3b-d). The specific surface area measured using BET evolved during cryomilling, increasing from 0.037 m^2/g for the spherical as-atomized particles to 0.44 m^2/g after 8 h of cryomilling (Table 1). For comparison, the theoretical surface areas of a smooth

sphere of 20-micron diameter and a disk of equal volume with a diameter of 100-micron are 0.025 m²/g and 0.32 m²/g, respectively. As cryomilling proceeds the surface area increases approximately linearly with time. Data from 16 h samples is not expected to follow the trend with the Pd-10Rh powder cryomilled for 8 h or less because cold welding occurs in these samples, thus limiting further increases in surface area. This observation from the data obtained using BET analysis was confirmed based on the SEM micrographs of the cross-sectioned particles seen in Figure 3.

Table 1. Powder and microstructural characteristics of atomized (as-atomized) and cryomilled Pd-10Rh powders (1h, 2h, 8h, and 16h refer to cryomilling times in hours). Crystallite size and microlattice strain determined from X-ray diffraction line profile analysis.

Powder	Surface area (m ² /g)	Crystallite size (nm)	Microlattice strain	Dislocation density (m ⁻²)
Atomized	0.037	230	0.002	1.2 x 10 ¹⁴
1h	0.088	270	0.012	5.6 x 10 ¹⁴
2h	0.13	130	0.010	1.0 x 10 ¹⁵
8h	0.44	77	0.014	2.4 x 10 ¹⁵
16h	0.031	29	0.014	2.35 x 10 ¹⁵
16h, BPR=64:1	0.045	25	0.032	1.6 x 10 ¹⁶

TEM observation of the atomized and cryomilled Pd-10Rh powder provides insight into the mechanisms responsible for the observed changes in microstructure caused by cryomilling.

The microstructure of the as-atomized particles appears compositionally homogenous with a small population of dislocations that formed during atomization and rapid solidification (Figure 3a) and with relatively few grain boundaries. However, Rh segregation on the secondary dendritic arms in the as-atomized Pd-10Rh was not observed as previously reported [7,6] due to overlapping of the Pd and Rh signals in TEM. Cryomilling generates dislocation tangles and sub-boundaries, as well as strain field contrast, all of which gradually intensify with increased milling time. These features are apparent in the micrographs shown in Figures 2b and 2c for powder cryomilled for 1 and 2 h, respectively. A large number of boundaries evolve during cryomilling, including elongated subgrains observed along the length of the particles. It was not possible to estimate the average length of the sub-grains by TEM due to a limited population of boundaries within a single particle. The width of the sub-grains after 1 and 2 h of cryomilling, however, was estimated to be approximately 400 nm and 300 nm, respectively. Cryomilling for 8 h led to further sub-grain refinement to approximately 100 nm (Figure 4d), while the length of the sub-grains was estimated to be around 1 μm. A high density of dislocations was observed in the interior of the grains after 8 h of cryomilling.

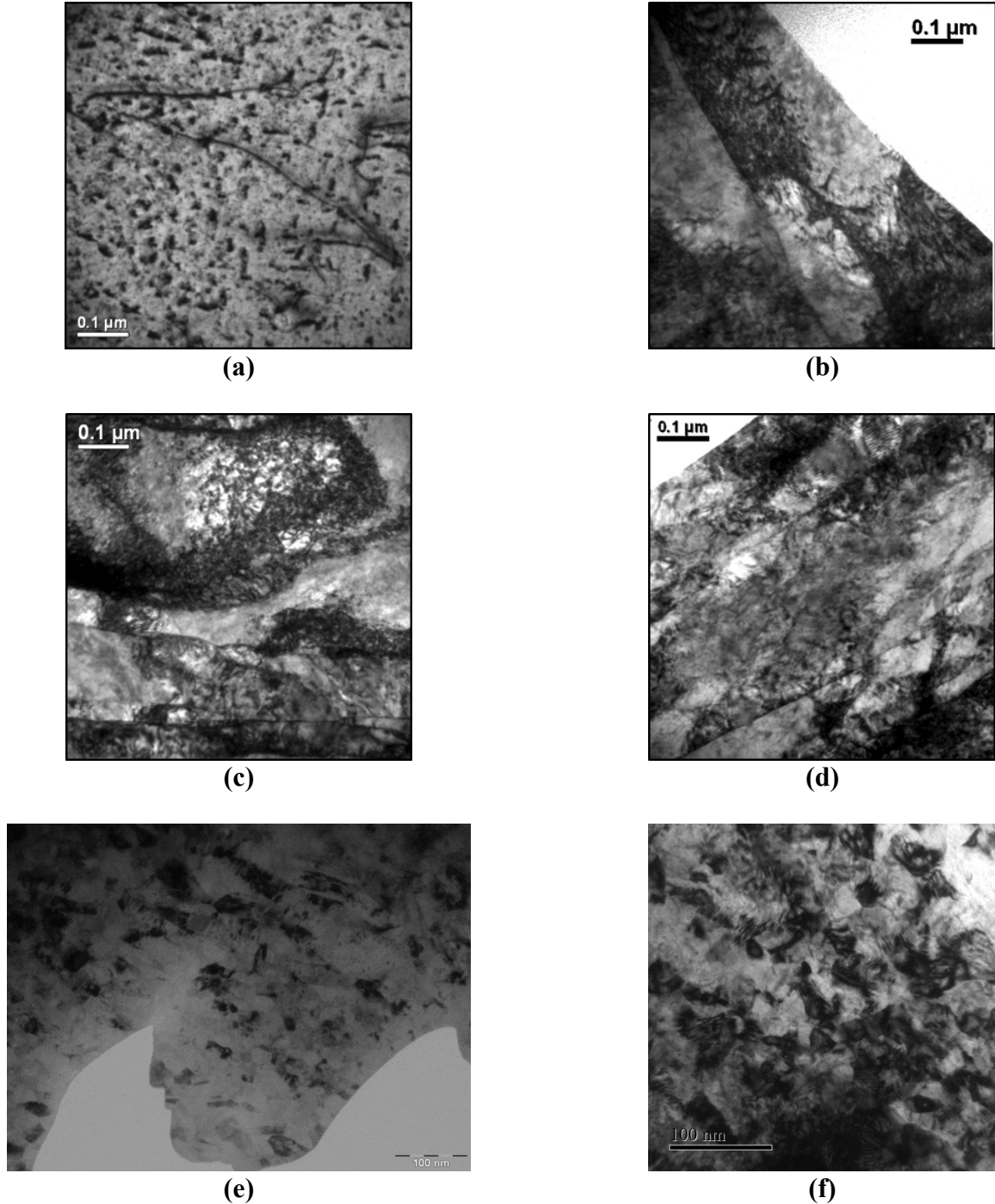


Figure 4. TEM micrographs of (a) atomized Pd-10Rh particles, and Pd-10Rh particles that were cryomilled for: (b) 1 h, (c) 2 h, (d) 8 h, (e) 16 h, and (f) 16 h, BPR=64:1.

In contrast, the samples cryomilled for 16 h (both BPR=32:1 and =64:1) exhibited fully developed microstructures. From the micrographs (Figure 4e and 4f), the boundaries are distinct in appearance, indicating that these are most likely high angle grain boundaries. Since the size of these grains is on the nanoscale, selected area diffraction to determine the misorientation

between two grains is nearly impossible. Additionally, dark field observation revealed that the presence of distinct grains indicating that the misorientation between grains must be large, i.e., high angle grain boundaries. The 32:1 sample had elongated grains, the width being 69.4nm \pm 29.3nm, and the length being 146.2nm \pm 67.8nm (aspect ratio \sim 3). In contrast, the 64:1 sample had equiaxed grains of an average diameter of 32.4nm \pm 16.9nm.

Phase identification and dislocation density were determined using XRD pattern analysis. The XRD pattern of the as-atomized powders confirms a solid solution in the starting Pd-10Rh alloy; moreover, the solid solution is maintained during cryomilling (Figure 5).

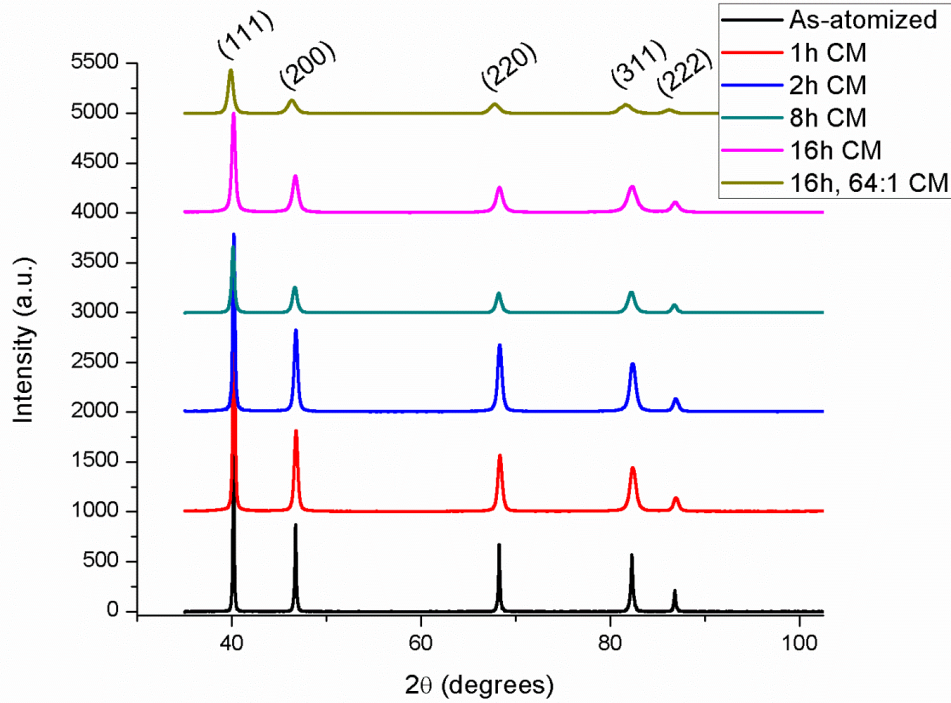


Figure 5. XRD patterns of atomized and cryomilled samples. Only the first five diffraction peaks are shown in this figure.

Rh segregation was again not observed in the as-atomized powders since it is on the order of only a few wt. percent, which is below the detection of XRD [7,6]. However, the peaks were shifted slightly towards higher angles as expected in a Pd-Rh solid solution alloy [8]. XRD peak broadening is observed with a trend of progressive broadening as cryomilling time is increased. This peak broadening can be attributed to microstructural refinement (a decrease in the size of subgrain structures, also called crystallites) and lattice strain induced by dislocations as reported by Ungár [9] and Zhao *et al.* [10,11]. In order to deconvolute crystallite size and strain-related broadening effects, the XRD patterns were analyzed using a simplified integral breadth method. The full width half maximum of each peak was measured using the Pearson VII function, and fitted according to a modified Williamson-Hall relationship [10,12]. The dislocation density ρ was then calculated from the following equation [11]:

$$\rho = \frac{2\sqrt{3}\langle \varepsilon^2 \rangle^{1/2}}{Db} \quad \text{Eq. [1]}$$

where lattice strain (ε) and crystallite size (D) were previously determined from the Williamson-Hall analysis [13], and b is the magnitude of the Burgers vector in the Pd-10Rh alloy (0.274 nm). The results of the XRD line profile analysis on the Pd-10Rh powder are summarized in Table 1, which shows clear trends of reduction in crystallite size, increased microlattice strain, and greater dislocation density with increasing cryomilling time. In particular, cryomilling leads to gradual refinement of the subgrain structure with increased milling time: from 230 nm for the as-atomized powder to 30 nm after 16 h of cryomilling. Additional XRD line profile analysis showed that the sample cryomilled for 16h using a 64:1 BPR had an increased grain size as well as an increased dislocation density. These values obtained from the XRD analysis do not agree with TEM results; however, this discrepancy can be attributed to the fact that XRD measures the coherent crystallite areas as grains, e.g., sub-grains are detected as distinct grains. Additionally, difficulties in deconvoluting individual contributions of grain size effects and dislocation densities on the broadening of the diffraction peaks could also contribute to differences between the TEM and XRD data.

Even though dislocations tend to migrate to grain boundaries or dislocation substructures under the applied strain experienced during milling, there is still a high concentration of residual dislocations located within the interior of the subgrains [14]. Zhao et al. found that in mechanically milled Fe and Cu, the dislocation densities measured using XRD profile analysis increased from $\sim 10^{14} \text{ m}^{-2}$ to $\sim 10^{15} \text{ m}^{-2}$ after similar milling times [10,11]. In the present study, the dislocation density measured by XRD increased with longer cryomilling time, from $1.2 \times 10^{14} \text{ m}^{-2}$ in the atomized powder to $2.4 \times 10^{15} \text{ m}^{-2}$ after 8 h of cryomilling; the presence of a high concentration of dislocations is also apparent in TEM micrographs (Figure 4). After 16 h of cryomilling, the dislocation density is lower in comparison to the sample cryomilled for 8 h; this is perhaps due to the fact that dislocations have been annihilated during the grain refinement processes. In addition to the strain contrast created by dispersed dislocations, dense dislocation walls are observed in the TEM micrographs in Figures 4b and 4c. In the 64:1 sample, the dislocation density was measured to be $\sim 10^{16} \text{ m}^{-2}$, two orders of magnitude greater than that of the atomized sample. This value was also substantiated by the TEM micrograph for the corresponding sample; however, the value could also represent an upper bound value due to the high concentration of grain boundaries also present in the sample.

In addition to grain size and dislocation density, the lattice parameter of each sample was measured using Bragg's law X-ray analysis. In theory, the lattice parameter of the Pd-10Rh should remain approximately constant even with increasing amounts of deformation; minor deviations may arise from instrumental variations and deformation provided that the material remains crystalline. As it can be seen previously in Table 1, the lattice parameter of the cryomilled Pd-10Rh changes slightly ($\leq 0.1\%$) with increased amounts of cryomilling. However, the lattice parameter of the final sample (BPR=64:1) increased by nearly 0.4%. This finding was later confirmed by obtaining an electron diffraction pattern from TEM. The exact cause of this lattice parameter expansion is still unknown at the time of this writing, and should be further investigated.

PC isotherms, shown in Figure 6, are used to compare the hydrogen storage characteristics of the different Pd-10Rh powders.

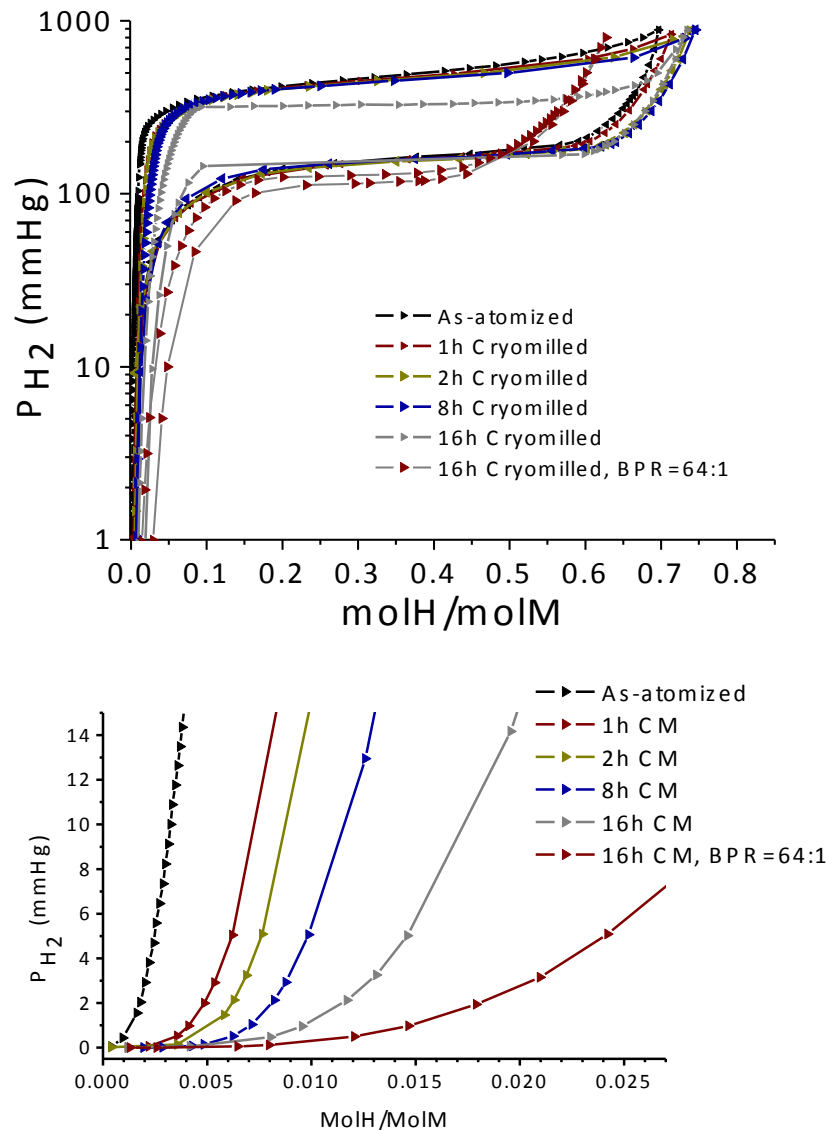


Figure 6. PC isotherms for as-atomized and cryomilled samples at (a) full range of molar H/M ratios and (b) low H/M ratios.

At very low pressure, hydrogen is soluble in the defect structure of the Pd-10Rh alloy (especially at free surfaces) and characterized by the H concentration extrapolated to zero pressure; this value is referred to as θ_{\max} . The conventionally-defined α -hydride phase, which exists at low concentrations of H, is characterized by a maximum concentration of H denoted α_{\max} and defined as the intersection of extrapolations of the low-pressure portion of the PC isotherm and the plateau portion of the PC isotherm. The plateau pressure, which represents the transformation of the α -phase solid solution to the β -hydride ($\alpha \rightarrow \beta$), has a slightly positive slope for these materials, thus the transformation in these materials occurs over a range of pressure (albeit a small range). The minimum H concentration of single-phase β -hydride (β_{\min}) is difficult to establish from the PC isotherms, but appears to differ for the different powders. For the purposes of comparing the powders at high H concentration, the equilibrium H concentrations (c_H) at pressure of 600 Torr and 760 Torr are used to demonstrate the differences between the different

powders. The concentrations of these transitions (θ_{\max} , α_{\max} , and c_H) are summarized in Table 2 for each powder.

The rates of H uptake for the different cryomilling times were calculated by normalizing the instantaneous H/M molar ratio with the equilibrium H/M molar ratio, and plotting as a function of time (Figure 7).

Table 2. Hydrogen uptake and solubility characteristics of atomized and cryomilled Pd-10Rh powders (1h, 2h, 8h, and 16h refer to cryomilling times in hours)

Powder	θ_{\max} (H/M)	α_{\max} (H/M)	c_H [P=600 torr] (H/M)	c_H [P=760 torr] (H/M)	Absorption half-life (sec)
atomized	0.002	0.046	0.54	0.66	88
1h	0.006	0.050	0.60	0.69	28
2h	0.008	0.057	0.62	0.71	42
8h	0.010	0.070	0.65	0.72	8
16h	0.015	0.070	0.65	0.72	50
16h, BPR=64:1	0.023	0.14	0.57	0.62	6

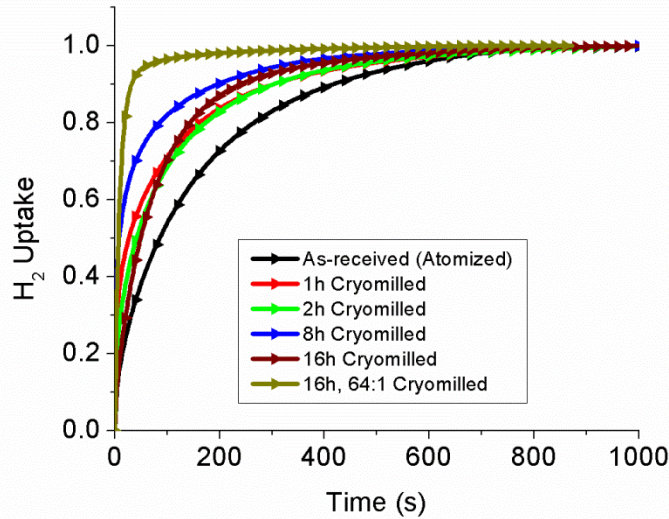


Figure 7. H uptake kinetics for atomized and cryomilled Pd-10Rh samples

The half-life of the H uptake process is compared in Table 3 for each cryomilling condition. The cryomilled powders absorb hydrogen faster than the atomized powder, by a factor of 3 and 2 for the powders that were cryomilled for 1 h and 2 h, respectively. Absorption was 10 times faster for the powder that was cryomilled for 8 h. Interestingly, the rate of absorption for the Pd-10Rh cryomilled for 16 h does not follow the hypothesized trend. Initially, the rate of absorption in the 16 h cryomilled sample is slower than the other cryomilled samples. After the H absorption

process exceeds 60% completion, the rate of absorption then increases to be faster than the samples cryomilled for 1 h and 2 h. The kinetics of absorption for the sample cryomilled for 16 h using a BPR of 64:1 tracked closer to that of the 8 h sample.

4. DISCUSSION

Microstructural evolution

The changes of various microstructural characteristics of the particles during cryomilling can be roughly divided into that which occurs on the macroscopic level, and that which occurs on the microscopic level. Thus, the changes in the powder after cryomilling will be described in a similar manner.

Macroscopic evolution

The macroscopic development of the cryomilled particles refers to the changes in particle morphology as a function of cryomilling time. The feedstock (as-atomized) powder begins as spherical powder, but it can be seen through the micrographs presented in the previous chapter that the particles change drastically with cryomilling. During the cryomilling process, the particles undergo cold welding, folding, and fracture. As previously noted, cold welding does not appear to be occurring in an observable frequency in the powder cryomilled up to 8h. Additionally, folding of the particles also does not appear to occur, and fracture of the particles only appears at the edges. This can be expected as Pd is a rather ductile material with the ability to accommodate significant plastic deformation [15]. Rh does not have a significant role on the mechanical behavior of the Pd-10Rh alloy, since Pd and Rh have similar atomic radii (0.134 nm for Rh versus 0.137 nm for Pd) [16]. In Pd powder cryomilled for 16h, the particles do exhibit signs of cold welding (as evidenced by the cross section micrographs). Folding again does not appear to play a significant role in the deformation of the particles, but fracture is most prevalent when a higher BPR is used. The lack of or increased presence of certain morphological features of the powder can be attributed to the manner in which the particles interacted with the slurry during cryomilling. Since Pd-10Rh has a high density (12.55 g/cm³), the particles are less likely to be disturbed by the turbulent flow of the cryogenic slurry. Additionally, it is reasonable to expect that the powder cryomilled using a higher BPR experiences a higher degree of deformation [17], fracture can be expected to play a more predominant role in the macroscopic evolution.

Microscopic evolution

Witkin and Lavernia [18] described microstructural refinement in materials processed using ball milling techniques (including cryomilling) as similar to that of materials processed using other types of bulk SPD techniques, such as ECAP, high pressure torsion, and cold rolling. The microstructural refinement observed in the cryomilled Pd-10Rh particles is similar to the plasticity-induced grain refinement that is observed in other face-centered cubic metals, such as Cu [14,19,20]. During severe plastic deformation, dislocations are nucleated in the material and move under the influence of the applied shear stresses. Once a high enough concentration of dislocations have formed, they can entangle to form dislocation substructures, annihilate [19], or migrate to boundaries and contribute to misorientation of these boundaries [20]. The continued nucleation and interaction of dislocations with further deformation subdivides grains and subgrains resulting in the microstructural refinement process [19]. The characteristic dimensions of the microstructure are reduced with continued cryomilling until the grain size saturates at a

minimum value, which is dependent on several material parameters including stacking fault energy, equilibrium distance between two edge dislocations, milling temperature, and composition [21–23]. However, no evidence of microstructural saturation, including equiaxed grains and a high concentration of high angle grain boundaries, was observed for cryomilling times up to 8 h in Pd-10Rh, suggesting that smaller sub-grain sizes can be achieved.

Indeed, smaller grains were achieved in the samples cryomilled for 16h, as evidenced by the apparent absence of dislocation cells and sub-boundaries. Additionally, the increased strain energy introduced to the powder cryomilled using a BPR of 64:1 yielded an even smaller grain size, which approaches minimum grain size values reported in Refs. [21,24]. However, one must note that when compared to other fcc materials which have been cryomilled, Pd-10Rh took a significantly longer time to reach a saturated microstructure. In contrast, Al requires only 8 h of cryomilling to reach an equilibrated rate of microstructural evolution [18]. A common parameter that many investigators have thought to be important in determining the refinement behavior of materials is the stacking fault energy of the milled material [18,24,25]. Both Pd and Al have high stacking fault energies, which cannot entirely explain the discrepancy in the milling time required to obtain a refined microstructure. However, stacking fault energy mostly indicates that dislocation activity rather than deformation twinning is the primary deformation mechanism even at small grain sizes. Closer inspection of Mohamed’s dislocation based model for the minimum grain size achieved through ball milling [21] reveals some insight for such differences in milling behavior. Mohamed defines the rate of grain refinement as:

$$\left(\frac{\delta d}{\delta t}\right)^{-} = A_1 \left[\left(\frac{\sigma}{G}\right)^{11} \left(\frac{L}{b}\right)^6\right] v_o C_v^\epsilon \exp\left(-\frac{aQ}{RT}\right) \quad \text{Eq. [2]}$$

Here, we can see that of the materials parameters (where G is the shear modulus of the material and b is the Burgers vector), G most strongly influences the rate of grain refinement as it is to the 11th power. Physically, this is an indication of the amount of deformation required to move dislocations through shear forces. Pd has a significantly larger shear modulus (45 GPa) compared to Al (26.2 GPa). Accordingly, it is reasonable to expect that it will take a significantly longer time to saturate the rate of grain refinement during ball milling of Pd than of Al. These theoretical insights are in good agreement with experimental observations.

As of the time of this writing, the origin of the anomalous lattice expansion of the 16h, 64:1 sample has not been determined. A similar lattice parameter expansion was reported by Lutterotti and Gialanella [26] in a ball milled Ni₃Al intermetallic powder and was attributed to the agglomeration of vacancies and antisite point defects. However, their findings cannot be used to explain our results, since the presence of antisite point defects along with the difference in atomic radii of Ni and Al can be used to explain the lattice expansion. Such expansion was not reported in alloy systems severely deformed using other solid state SPD techniques. However, possible explanations for this effect could arise from the relatively high defect (primarily grain boundaries and dislocations) concentration of the 16h, 64:1 sample. The origin of this effect should be studied in greater detail.

Hydrogen sorption properties

There are several aspects of hydrogen sorption properties which can be studied. In the present manuscript, we choose to primarily focus on properties derived from characteristics of the PC

isotherm, and how they relate to the microstructural properties observed in the as-atomized and cryomilled Pd-10Rh. These properties include the surface area effects, dislocation based effects, grain boundary based effects, and H sorption hysteresis effects.

Surface area effects on the PC isotherm

At very low pressure, differences in hydrogen uptake are apparent for the atomized and cryomilled samples as characterized by θ_{\max} . Because the large, negative heat of chemisorption is greater than the heat of absorption, the lag at very low pressure (dilute concentrations) must correspond to occupation of surface and sub-surface sites as well as other traps such as vacancies, grain boundaries and dislocations [27]. The surfaces, in particular, can act as low pressure traps for hydrogen, adsorbing hydrogen to the surface of the particle before being absorbed into the material [28]. The parameters θ_{\max} and α_{\max} are plotted in Figure 8 as a function of BET surface area, showing approximately exponential or linear trends between surface area and hydrogen concentration for both parameters.

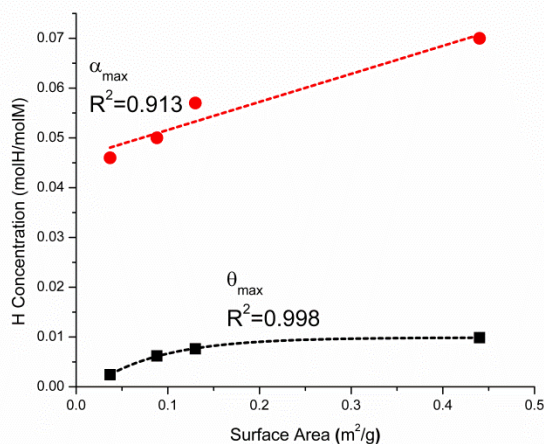


Figure 8. α_{\max} and θ_{\max} as a function of specific surface area.

Figure 8 shows that these trends can be demonstrated for the Pd-10Rh cryomilled up to 8 h. However, the trends do not follow for both samples cryomilled for 16 h (omitted in this figure), as particularly α_{\max} and increases while the particle surface area decreases. The particle surface area of the Pd-10Rh decreases primarily because cold welding becomes operative between 8h and 16h of cryomilling. Although it is intuitive to believe θ_{\max} and surface area are related, the apparent exponential relationship between these parameters implies a more complex connection. Determination between θ_{\max} and surface area will require more careful investigation.

Dislocation-based effects on the PC isotherm

While it seems reasonable to attribute the increase in θ_{\max} to greater surface area, the correlation between surface area and α_{\max} makes less physical sense. In the case of α_{\max} , the bulk alloy (rather than surface) must interact with hydrogen, as implied by the magnitude of the hydrogen concentration. Additionally, although perhaps a portion of the increase of α_{\max} is related to surface area, the greater slope of the concentration-surface area curve in the case of α_{\max} compared to θ_{\max} (Figure 8) suggests another explanation. Comparison of θ_{\max} and α_{\max} to the dislocation density measured by XRD in Figure 9 shows that there is a greater correlation between α_{\max} and the dislocation density than the particle surface area.

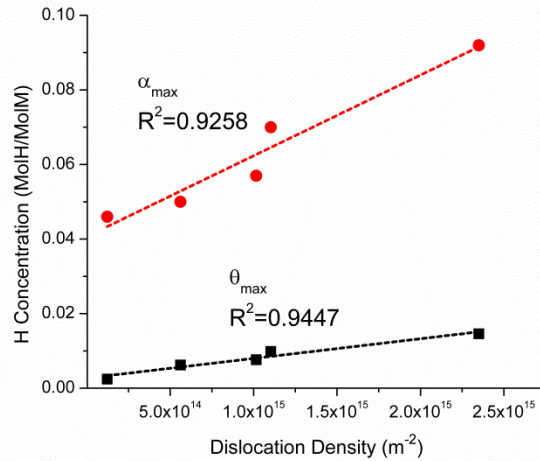


Figure 9. Comparison of α_{\max} and θ_{\max} as a function of dislocation density.

Indeed, highly cold worked Pd exhibited solubility enhancements at low H concentrations, increasing the measured α_{\max} phase [29–32]. The increase of θ_{\max} as a function of increasing dislocation density can be expected because θ_{\max} depends on the concentration of defects (mostly dislocations and grain boundaries) at the sub surface of the Pd-10Rh [27].

Grain size effects on the PC isotherm

Finally, θ_{\max} and α_{\max} were plotted as a function of the inverse grain size D^{-1} in Figure 10. θ_{\max} trended upwards with decreasing grain size, following a similar logic to the relationship between θ_{\max} and dislocation density. The frequency of grain boundaries located at the sub surface should be higher if the average grain size is smaller. Increasing α_{\max} values also correlated well with the decrease of the average grain size, and is in agreement with other literature on the subject [33–36]. However, the relationships between α_{\max} , grain size, and dislocation density appear to be interrelated. A review of the literature does not specifically elucidate whether increases in α -phase solubility in Pd are more strongly related to increases in dislocation density or decreases in average grain size. It should be noted though that in many of these relevant studies, the bulk Pd was plastically deformed to relatively high strains with the purpose of introducing high dislocation densities [29,30,32,37]; it is certainly possible that grain refinement occurred during these processes. Interestingly, the post deformation microstructure was never characterized in these studies.

While many previous studies also examined nanocrystalline Pd and its hydrogen sorption, those investigations used materials whose grain sizes were significantly smaller than those shown here in the present work (<10 nm versus 150-200 nm). This implies that between these two average grain size regimes, there is a change in H sorption mechanisms. The reasons for this apparent transition of behavior have not been described yet in literature, and will be investigated in the future.

Through the course of the microstructural investigation, the 16h BPR=64:1 sample was found to have an expanded lattice parameter. It is well known that hydrogen is drawn to regions of tensile stress, while being repelled by regions of compressive stress. It stands to reason that if the cause of the change in lattice parameter is due to a stress related by nature (including dislocations and grain boundaries evolved from dislocation mediated processes), then changes in PC isotherm

behavior could also be related to the dilatation. Again, this hypothesis must be further investigated.

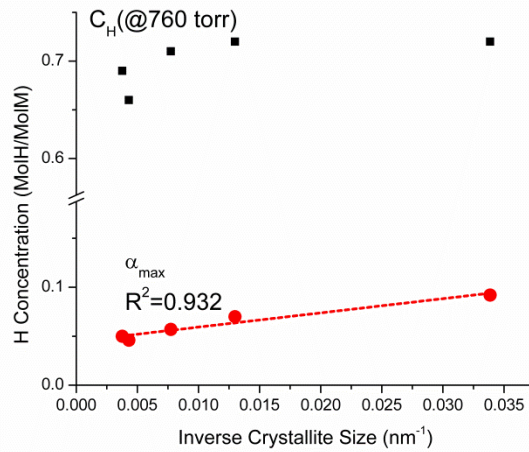


Figure 10. Comparison of α_{\max} and θ_{\max} as a function of inverse grain size (nm^{-1}).

Hysteresis and its relationship to microstructure

The hysteresis in the PC isotherms is attributed to dislocation generation during hydrogen absorption/desorption as described in Ref. [38]. The observation that the size of the hysteresis loop is not a function of the cryomilling is consistent with unsaturated dislocation structures (and the continuous evolution of dislocation density with cryomilling time, Table 2). In contrast, if dislocation structures are saturated, resistance to formation of additional dislocation structures may impede phase transformations, thus affecting hysteresis. A sloping plateau pressure has been previously attributed to several factors in alloys and intermetallics, including compositional inhomogeneity in the sample [39,40]. In the cryomilled samples, the slope of the plateau is reduced with longer cryomilling time, which suggests a reduction of the inherent segregation in the Pd-Rh solid solution. Longer cryomilling time refines the microstructure, effectively decreasing the secondary dendrite arm spacing relative to the original solidified microstructure. While the atomized powder for this study was selected to have minimal segregation [7,6], some segregation in the atomized powder likely exists, although compositional segregation was not detected in the atomized or cryomilled powders. A plateau that varies between about 300 and 600 Torr is observed here, which agrees well with previous studies on hydrogen absorption in Pd-10Rh alloys [41]. In addition to the sloping pressure plateau, a large increase in the pressure of the plateau region is observed for the Pd-10Rh alloy compared to pure Pd. Previous work has attributed the increased plateau pressure to lattice contraction upon alloying and the additional strain energy that must be overcome as hydrogen occupies octahedral sites [41]. This interpretation can be extended to understand the decrease in pressure of the plateau for longer cryomilling times, while maintaining the overall features of the PC isotherms. The internal strain (Table 2) that is introduced during the cryomilling process is essentially a dilation of the lattice, opposing the effect of alloying. In other words, greater lattice strain due to longer cryomilling times flattens the pressure plateau by offsetting lattice contraction associated with alloying.

Hydrogen uptake kinetics and its relationship to microstructure

The rates of H uptake for the different cryomilling times were calculated by normalizing the instantaneous H/M molar ratio with the equilibrium H/M molar ratio, and plotting as a function of time (Figure 7). The half-life of the H uptake process is compared in Table 2 of the previous chapter for each cryomilling condition. The cryomilled powders absorb hydrogen faster than the atomized powder, by a factor of 3 and 2 for the powders that were cryomilled for 1 h and 2 h, respectively. Absorption was 10 times faster for the powder that was cryomilled for 8 h. The rate-limiting step in the hydrogen absorption process in Pd is still debated [42]. Three elementary steps are generally considered in the mechanism of absorption of hydrogen gas into a metal lattice: (i) dissociative chemisorption, (ii) absorption from the surface into subsurface sites, and (iii) bulk diffusion [43]. The increased rates of hydrogen absorption with greater cryomilling time observed in the present study can be explained by the increase in surface area-to-volume ratio if either chemisorption or transfer to subsurface sites is rate-limiting. If diffusion is rate limiting, then rates of hydrogen uptake will be controlled, in part, by the minimum dimension of the particulate, in this case the thickness of the flattened cryomilled particles. Since we idealize the particles as continuously flattened during cryomilling, the relative thickness scales approximately with the surface area. Thus, regardless of the kinetic pathway, to first order the rate of hydrogen uptake should scale with the specific surface area, which is plotted in Figure 8. While there is a general trend of shorter uptake times for greater surface area, the samples cryomilled for 1 and 2 h are not self-consistent in this regard. There is no clear explanation for this apparent inconsistency; morphologically (Figures 2 and 3) the powders cryomilled for 1 and 2 h respectively are very similar except that longer cryomilling time results in thinner disks of larger diameter. However, there are likely competing factors in the process of uptake, such as the role of microstructural defects on the diffusive transport of H in the bulk. H trapping, for example, impedes bulk diffusion, thus high density of hydrogen traps (such as dislocations or grain boundaries) can, in principle, reduce the apparent diffusivity and limit rates of uptake. Longer cryomilling times or higher-energy milling conditions (e.g., more milling media) could conceivably result in microstructures that promote diffusion-limited processes that reduce the rate of hydrogen uptake. This appears to be the case for the sample cryomilled for 16h.

On the other hand, particle morphologies and microstructures created through cryomilling could also both contribute towards even faster rates of hydrogen absorption, as demonstrated by the 16h BPR=64:1 sample. The half-life of absorption in this sample is even faster than that of the sample cryomilled only for 8h despite having significantly less surface area and thicker particle widths. In this case, there must be another factor which influences the rate of absorption, since neither physical property indicates that either adsorption or bulk diffusion act as the rate limiting step. Figure 11 shows the relationships between parameters, which appear to influence the rate of hydrogen absorption in cryomilled Pd-10Rh.

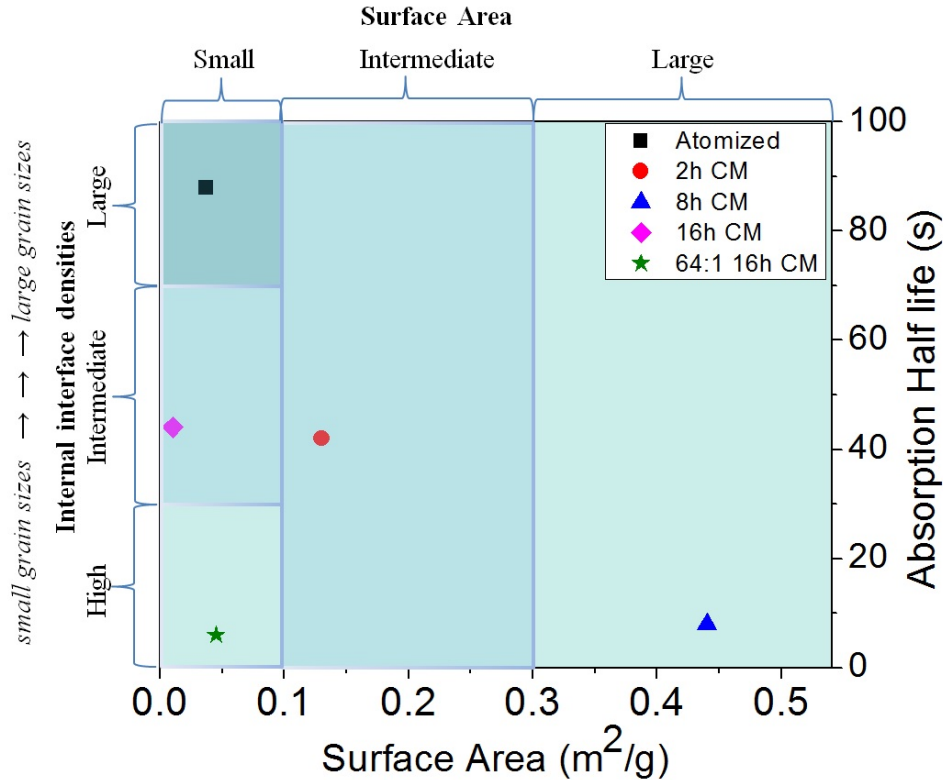


Figure 11. Comparison of specific surface area and hydrogen absorption half-life of atomized and cryomilled Pd-10Rh.

At the surface of the particles, a high density of defects could change kinetics of dissociative chemisorption and absorption into subsurface sites. In the bulk, while certain grain boundaries and dislocations can impede bulk diffusion, others could possibly provide regions of enhanced diffusion. In the 16h BPR=64:1 sample, the frequency of diffusion enhancing defects is certainly feasible given the high concentration of grain boundaries and dislocations present in the material.

5. ANTICIPATED IMPACT

While there are several issues which remain to be addressed in regards to the effects of hydrogen in metals, the present study provides some insight towards understanding of the cryomilling process and its effects on Pd-10Rh microstructure, and in turn microstructural effects on H sorption behavior. The investigation outlined by this report has two key findings which can be further studied: i) the hysteresis effect observed in the PC isotherms and microstructural characteristics which influence this phenomenon, ii) the relationship between microstructural properties and hydrogen absorption rates, and iii) desorption studies on cryomilled Pd-10Rh. From a technological perspective, both hysteresis effects as well as faster rates of absorption will be important for future applications in hydrogen storage materials. In both cases, understanding the material processing parameters which can create “engineered” microstructures designed for certain hydrogen storage properties will be important towards knowledge for application.

Much remains to be understood about hysteresis effects in hydrogen sorption in Pd-10Rh. In particular, the specific microstructural characteristics, which govern hysteresis effects are not well known. In the present investigation, it has been hypothesized that a material’s ability to plastically deform (e.g., to nucleate/move dislocations) is directly related to the occurrence of

absorption/desorption hysteresis. The 16h, BPR=64:1 sample, which had a microstructure where further dislocation nucleation and movement were impeded, also exhibited a decreased absorption/ desorption hysteresis. Further studies to test this hypothesis could be pursued in earnest in forthcoming programs. While we have investigated one possible route for decreasing hysteresis, other strategies of limiting dislocation activity could be pursued. For example, synthesis of Pd-oxide ceramic composites could be used to leverage some knowledge about hysteresis effects.

As mentioned previously, the exact mechanisms behind the increased rates of absorption observed in the Pd-10Rh sample cryomilled for 16h, BPR=64:1 have not been ascertained. In this report, we hypothesized that such differences could be related to the presence of many grain boundaries, especially near the surfaces of particles. While it is unlikely that such a study can be undertaken from a purely experimental perspective, first principles modeling and simulation may be able to provide some insight into the role of grain boundaries in the absorption process. Furthermore, information from these studies then may be used in larger constitutive modeling efforts to verify experimental data.

While much effort has been devoted to the hydrogen absorption processes in cryomilled Pd-10Rh, there has been no effort as of yet concerning the rates of hydrogen desorption from these materials. Understanding of this particular property would be useful from a technological perspective if cryomilled Pd-10Rh is to be used in hydrogen storage applications, where release of the hydrogen will be just as important as the absorption step. Hydrogen desorption experiments could be carried out in equipment similar to that which was used to record absorption data in this study.

6. CONCLUSIONS

In the present work, Pd-10Rh was cryomilled, and the microstructures created through the process were investigated. Cryomilling was found to flatten the once round as-atomized particles, as well as introduce a large density of defects such as dislocations and grain boundaries. Through the course of the cryomilling process, the particles became flatter, and dislocation sub structures were observed in the microstructure. After 8 h of cryomilling, the particles reached their minimum thickness, and elongated grains approximately 100 nm in width and several micrometers long were observed in the microstructure of the sample. However, after 16 h of cryomilling cold welding began to occur, causing the particles to become thicker and shorter. Elongated grains ~50 nm in width and ~150 nm in length were observed. An additional cryomilling experiment was also performed by using a ball-to-powder ratio of 64:1, introducing even more strain into the powder during the cryomilling process. The microstructure of this sample was more uniform with equiaxed grains, with an average size of approximately 30 nm in diameter. It was theorized that the microstructural refinement behavior of Pd-10Rh was due to its high bulk modulus compared to other high stacking fault materials such as Al.

The H sorption properties of the Pd-10Rh powders were also measured. The deformation induced by cryomilling did affect some absorption properties, including increasing α -phase solubility and θ_{\max} , a parameter used to measure interactions with surface defects at low H concentrations. The changes in these parameters were attributed to the increased dislocation densities caused by cryomilling. The overall capacity of the Pd-10Rh powders milled up to 16 h using a BPR of 32:1 were unaffected, despite the average grain sizes of these samples having been reduced to hundreds of nanometers. The Pd-10Rh sample, which was exposed to higher

amounts of deformation (cryomilled for 16 h using a BPR=64:1), did exhibit a reduced capacity consistent with other Pd samples reported in literature whose average grain size was less than 50 nm. These results imply that there is a transition in H sorption behavior as related to average grain size when the grain size is between 50 and 100 nm. Finally, the kinetics of some of the cryomilled Pd-10Rh material was studied. The rates of absorption increased in samples, which had been exposed to more strain from cryomilling. This was observed in samples cryomilled up to 8 h, and was associated with the presence of dislocation sub structures which could act as pathways for fast diffusion. However, in the sample with a more refined microstructure (i.e., Pd-10Rh cryomilled for 16 h), absorption initially was slower than the other cryomilled material, but then increased. This behavior is hypothesized to have been caused by a high density of trapping sites located within the grain boundaries.

7. REFERENCES

- [1] Fuel Cell Technologies Office: Hydrogen Storage, accessed 6 Apr. 2013.
URL: <http://www1.eere.energy.gov/hydrogenandfuelcells/storage/index.html>.
- [2] Léon A. Hydrogen Storage, in: Léon A (Ed.). *Hydrog. Technol.* Springer Berlin Heidelberg; 2008.
- [3] Valiev R. *Nat Mater* 2004;3:511.
- [4] Hull D, Bacon DJ. *Introduction to Dislocations.* Elsevier; 2011.
- [5] Weertman J, Weertman JR. *Elementary Dislocation Theory.* Oxford University Press; 1992.
- [6] Yang NYC, Ong MD, Lavernia EJ. *Material Synthesis and Hydrogen Storage of Palladium-Rhodium Alloy.* Sandia National Laboratories; 2011.
- [7] Yang N, Guthrie S, Ho S, Lavernia E. *J Mater Sci* 1997;32:6589.
- [8] n.d.
- [9] Ungár T. *Adv Eng Mater* 2003;5:323.
- [10] Zhao Y., Sheng H., Lu K. *Acta Mater* 2001;49:365.
- [11] Zhao YH, Lu K, Zhang K. *Phys Rev B* 2002;66:085404.
- [12] Zhao YH, Zhang K, Lu K. *Phys Rev B* 1997;56:14322.
- [13] Williamson G., Hall W. *Acta Metall* 1953;1:22.
- [14] Edalati K, Fujioka T, Horita Z. *Mater Sci Eng A* 2008;497:168.
- [15] Sanders PG, Eastman JA, Weertman JR. *Acta Mater* 1997;45:4019.
- [16] Wise EM. *Palladium: Recovery, Properties, and Uses.* New York: Academic Press; 1968.
- [17] Lin Y, Yao B, Zhang Z, Li Y, Sohn Y, Schoenung J, Lavernia E. *Metall Mater Trans A* 2012;43:4247.
- [18] Witkin DB, Lavernia EJ. *Prog Mater Sci* 2006;51:1.
- [19] Wang K, Tao NR, Liu G, Lu J, Lu K. *Acta Mater* 2006;54:5281.
- [20] Mishra A, Kad BK, Gregori F, Meyers MA. *Acta Mater* 2007;55:13.
- [21] Mohamed FA. *Acta Mater* 2003;51:4107.
- [22] Eckert J, Holzer J c., Krill C e., Johnson W l. *J Mater Res* 1992;7:1751.
- [23] Pippin R, Wetscher F, Hafok M, Vorhauer A, Sabirov I. *Adv Eng Mater* 2006;8:1046.
- [24] Fecht H-J. *Nanostructured Mater* 1995;6:33.
- [25] Suryanarayana C. *Prog Mater Sci* 2001;46:1.
- [26] Lutterotti L, Gialanella S. *Acta Mater* 1998;46:101.
- [27] Flanagan TB, Luo S, Wang D. *The Effect of Substitutional Alloying on the Hydrogen Solubilities in Palladium*, in: *Electrochem. Soc. Proc.*, vol. 97-16. n.d.
- [28] Powell GL, Kirkpatrick JR, Conant JW. *J Common Met* 1991;172-174, Part B:867.
- [29] Flanagan TB, Lynch JF, Clewley JD, Von Turkovich B. *J Common Met* 1976;49:13.
- [30] Flanagan TB, Lynch J. *J Common Met* September;49:25.
- [31] Kirchheim R. *Acta Metall* 1982;30:1069.
- [32] Kirchheim R. *Acta Metall* 1981;29:835.
- [33] Kirchheim R, Mütschele T, Kieninger W, Gleiter H, Birringer R, Koblé TD. *Mater Sci Eng* 1988;99:457.
- [34] Mütschele T, Kirchheim R. *Scr Metall* 1987;21:135.
- [35] Kuji T, Matsumura Y, Uchida H, Aizawa T. *J Alloys Compd* 2002;330-332:718.
- [36] Eastman JA, Thompson LJ, Kestel BJ. *Phys Rev B* 1993;48:84.
- [37] Maxelon M, Pundt A, Pyckhout-Hintzen W, Kirchheim R. *Scr Mater* 2001;44:817.

- [38] Cappillino PJ, Lavernia EJ, Ong MD, Wolfer WG, Yang NY. *J Alloys Compd* 2014;586:59.
- [39] Park C-N, Luo S, Flanagan TB. *J Alloys Compd* 2004;384:203.
- [40] Luo S, Park C-N, Flanagan TB. *J Alloys Compd* 2004;384:208.
- [41] Fazle Kibria AKM, Sakamoto Y. *Int J Hydrog Energy* 2000;25:853.
- [42] Delmelle R, Proost J. *Phys Chem Chem Phys* 2011;13:11412.
- [43] Okuyama H, Siga W, Takagi N, Nishijima M, Aruga T. *Surf Sci* 1998;401:344.

Distribution

1 MS0899 Technical Library 9536 (electronic copy)

